Materials Science and Engineering A 499 (2009) 507–517

Contents lists available at ScienceDirect

Materials Science and Engineering A

journal homepage: www.elsevier.com/locate/msea

Processing, compression response and finite element modeling of syntactic foam based interpenetrating phase composite (IPC)

Rahul Jhaver, Hareesh Tippur*

Department of Mechanical Engineering, Auburn University, Auburn, AL 36849, United States

ARTICLE INFO

Article history:
Received 22 July 2008
Received in revised form 31 August 2008
Accepted 8 September 2008

Keywords:
Interpenetrating phase composite (IPC)
Co-continuous composite
Syntactic foam
Open-cell aluminum foam
Compression response
Stress–strain behavior
Finite element analysis

ABSTRACT

The feasibility of processing lightweight interpenetrating phase composite (IPC) foam is demonstrated. The composite is produced by infiltrating uncured epoxy-based syntactic foam into an open-cell aluminum preform, resulting in an IPC foam with improved compression characteristics relative to conventional syntactic foams. Different IPC foam varieties are prepared by varying the volume fraction of microballoons in the syntactic foam from 20% to 40% while keeping the volume fraction of the metallic network the same. Two variations of these IPC foam are produced using the aluminum preform in (a) 'as-is' condition and (b) after coating it with silane to increase adhesion between the metallic network and polymer foam. The IPC foam samples in general and the silane coated ones in particular show significant improvement in elastic modulus, yield stress and plateau stress values when compared to the corresponding syntactic foam of the same volume fraction of microballoons. The increase in plateau stress of IPC foam samples is about eight times that of an unfilled preform and approximately 42% higher than that of the corresponding syntactic foam. Up to 50% higher energy absorption by the silane treated IPC foam relative to the corresponding syntactic foam is also achieved. A Kelvin cell based 3-D elasto-plastic finite element model capable of capturing both linear and nonlinear characteristics of the IPC foams is also presented.

1. Introduction

Continued demand for lighter, stiffer, stronger and tougher structural components requires development of novel materials. Heterogeneous materials with discrete, dispersed and/or embedded phases in a matrix material (fiber reinforced composites, particulate composites, functionally graded materials, syntactic foams, etc.) are found suitable for many structural applications. There are, however, limitations in terms of the degree of concentration of the secondary phase that can be dispersed into the primary phase and the degree of inter connectivity between the phases. Nature overcomes these limitations by adopting 3-D interpenetrating microstructure as evident in skeletal tissue and botanical systems. This observation has inspired a relatively new category of materials called interpenetrating phase composite/s or IPC (also called co-continuous composites). The IPC are multiphase materials in which the constituent phases are interconnected three-dimensionally and topologically throughout the microstructure (and hence sometimes are referred to as "3–3" composites). That is, both matrix and reinforcement phase/s interpenetrate all over the microstructure in all the three spatial dimensions. Thereby the two constituents in their stand alone state would have an open-cell microstructure. Hence, *IPC are uniquely different from traditional composites comprising of a matrix with one or more reinforcing filler phases* (long fibers, whiskers, particles, microballoons, etc.) *where such a complete interpenetration does not occur*. Consequently, each phase of an IPC contributes its property to the overall macro scale characteristics synergistically. For example, if one constituent provides strength and toughness, the other might enhance stiffness, thermal stability, acoustic insulation and/or dielectric characteristics. Additionally, it is also possible to tailor residual stresses in the constituents to produce advantageous macro scale response in a metal–ceramic IPC. The tensile residual stresses in the metallic phase and compressive ones in the ceramic phase delays crack initiation and strengthens the IPC. Based on the occurrence of interpenetration at different length scales, interpenetrating phase composites can be classified as molecular, micro or meso varieties. A blend of two or more *cross-linked* polymers which are interlaced but not covalently bonded to each other and cannot be separated unless chemical bonds are broken is an example of a molecular scale IPC and is called an InterPenetrating Network (IPN).

Some of the conceptual underpinnings and possible material processing strategies for IPC are reviewed by Clarke [1]. The work by Breslin et al. [2] outlines material processing and characterization of aluminum/alumina IPC using a liquid phase displacement reaction method. The resulting IPC is shown to have excellent

* Corresponding author. Tel.: +1 334 844 3327.
E-mail address: htippur@eng.auburn.edu (H. Tippur).

0921-5093/$ – see front matter © 2008 Elsevier B.V. All rights reserved.
doi:10.1016/j.msea.2008.09.042

mass density, thermal conductivity and CTE characteristics without compromising stiffness or fracture toughness. The elastic–plastic behavior of this IPC is studied by Daehn et al. [3] using experimental and finite element methods. Polymer networks made by a photo-cross-linking method are reported by Imagawa and Qui [4]. Thermal expansion behavior of alumina/aluminum IPC is reported by Skirl et al. [5]. They used a pressure infiltration technique to introduce aluminum into slip cast and then sintered alumina. These authors suggest that tensile and compressive residual stresses in alumina and aluminum phases, respectively, contribute favorably to the overall thermal coefficient of expansion. They report an increase in failure strain as the metal content increases in the composite. Veenstra et al. [6] also developed polymer blends with interpenetrating microstructures and compared their mechanical properties to the ones based on the same polymers processed with a droplet/matrix morphology. A significantly higher tensile modulus without a notable drop in the tensile and impact strengths when compared to the one obtained from dispersed blends is reported. Finite element modeling of a two phase interpenetrating microstructures to study elastic, strength and thermal properties is reported by Wegner and Gibson [7]. An enhancement in thermo-mechanical characteristics in IPC is observed. In a recent work on graphite/aluminum IPC Etter et al. [8] examined flexural strength and fracture toughness at room temperature and at 300 °C. Their global measurements indicate a 200% improvement in both these characteristics for IPC over the un-infiltrated material at room temperature and at elevated temperatures no significant drop in properties is seen. Estimation of elastic properties of alumina/aluminum IPC structures using micromechanics approach is the focus of the work reported by Moon et al. [9]. Fatigue behavior of graphite/aluminum IPC is studied by Mayer and Papakyriacou [10]. They attempted to improve the low fracture toughness of polycrystalline graphite using infiltration by lightweight metals such as aluminum. A 30% increase in the cyclic strength and a 10% increase in the endurance limit are reported. Static compression and energy absorption of metal–polymer IPC are examined by Liu and Gong [11]. They infiltrate polyethylene or epoxy into an open-cell aluminum network to prepare IPC.

A class of structural foams called syntactic foams is considered for structural applications in recent years [16,17]. These foams can be distinguished from conventional variety by the way they are manufactured. Unlike traditional foams which are produced by gasification of the matrix material, syntactic foams are produced by mechanical blending of hollow polymer, ceramic or metal microballoons (hollow microspheres) in a polymer or metal matrix. Thus porosity is due to the 'filler' phase resulting in a closed-cell microstructure. Further distinction of these foams is that porosity in these materials is often microscopic and known to offer many advantages including high surface area to volume ratio as well as macroscopic isotropy. The range of engineering applications of these foams has increased in recent years due to the advancement of materials processing methods that offer choices in microballoon wall-thickness and diameter as well as the materials with which they are made of. Syntactic foams have been extensively used by naval and marine equipment manufacturers for decks and submarines buoys. They are also used in civil and industrial engineering as imitation wood and other building construction materials for their high shear stiffness and specific strength. Due to the high specific energy absorption and impact resistance, syntactic foams have the potential for use as core materials of sandwich structures. Syntactic foams made of glass and carbon micro-/nano-spheres are used in aerospace structures, missile heads and heat shields for space vehicles. They are also employed in electronics and telecommunications due to superior thermal and dielectric properties as well as shock absorption characteristics.

The compression response of polymer syntactic foams can be further enhanced by infiltrating the syntactic foam into lightweight open-cell preform/scaffold made of a stronger and tougher material such as an open-cell metal foam. The resulting composite foam could have improved mechanical characteristics in tension and shear when compared to the conventional polymer syntactic foams. Accordingly, in this paper the feasibility of processing polymer syntactic foam-aluminum foam IPC is demonstrated and its compression response is studied. In the following section, experimental details of material preparation are described. Mechanical characterization of syntactic foams and IPC foams is presented in Section 3. Relevant mechanical properties are compared in Section 4 and possible explanations for the differences are provided with the aid of microstructural analysis. In Section 5, a unit cell based finite element model capable of capturing the salient features of the experimental observations is presented. The results of this investigation are summarized in Section 6.

2. Material preparation

2.1. Syntactic foam preparation

Epoxy-based syntactic foams containing different volume fractions (20%, 30% and 40%) of hollow soda-lime glass microballoons were processed. The method involved heating epoxy resin to 50 °C for ~45 min. Predetermined amount of microballoons (spherical hollow balloons of mean diameter ~60 μm and wall-thickness ~600 nm) were added into epoxy resin and the mixture was carefully stirred ensuring uniform distribution of the filler. Subsequently, an amine based curing agent was introduced and stirring was continued. The mixture was then placed in a vacuum chamber and evacuated down to −75 kPa (gage) pressure. Once this pressure was reached the vacuum was released and the chamber was returned to atmospheric condition. This process was repeated (about 8–10 times) until no air bubbles were observed in the mixture. (This method of cyclic vacuuming of the mixture was found to be more effective when compared to holding the vacuum continuously for a set period of time.) When the mixture showed a tendency to gel, it was transferred into a silicone rubber mold with a blind cylindrical cavity. The increased viscosity of the mixture prevented segregation of microballoons due to buoyancy forces. The mixture was then cured at room temperature for a period of 48 h and rested for over a week to obtain a macroscopically homogeneous and isotropic solid. The cylindrical sample was then machined to the required dimensions. Unless specified otherwise, in this work, the sample length and diameter were 20 mm and 26.7 mm, respectively.

2.2. IPC foam preparation

Many different strategies have been proposed in the literature to process co-continuous composites including powder metallurgy [13], squeeze casting [14,8], stir casting [15], and molten metal infiltration [5]. In this work pressureless infiltration technique was used. Commercially available open-cell aluminum foam (made of Al 6101-T6; pore density = 40 ppi, relative density = 9%, manufactured by ERG Inc., USA) was used as the scaffold for the IPC foam. The preform has a uniform cell size distribution (Fig. 1(a)) resulting in an isotropic mechanical response at macro scales. The manufacturing of the IPC foam consisted of the following steps. A silicone rubber mold was first prepared with a blind cylindrical well of dimensions nearly close to the final sample dimensions. The syntactic foam (prepared as previously described) was then poured into the rubber mold just before the mixture started to gel. Subsequently

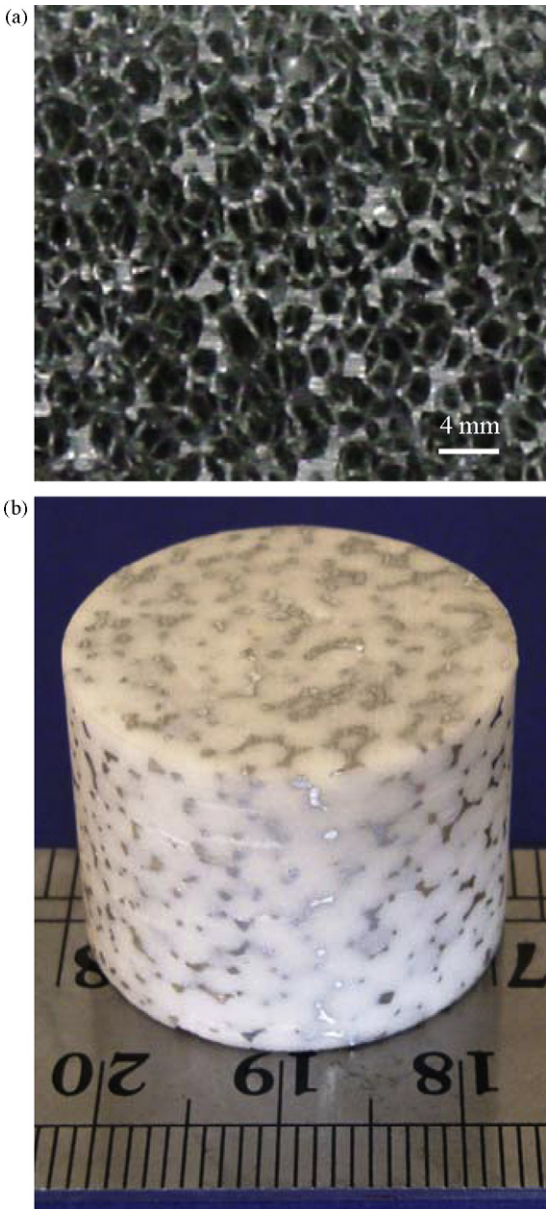

Fig. 1. Photograph of (a) 40 pores per inch open-cell aluminum preform/scaffold and (b) interpenetrating phase composite (IPC) foam made by infusing syntactic foam into the preform.

a cylindrical aluminum preform of the required dimensions was slowly lowered into the cavity previously filled with uncured syntactic foam. This ensured good percolation of the uncured syntactic foam mixture into all the cells of the preform. The resulting IPC foam was then cured at room temperature for 48 h before removing from the mold for machining. The cylindrical sample was subsequently machined to a length of 20 mm and diameter 26.7 mm (Fig. 1(b)).

Two different types of cylindrical IPC foam specimens were prepared. In the first type, the aluminum preform was used in 'as-is' state after degreasing it with laboratory grade alcohol. In the second type, the surface of the degreased aluminum preform was coated with amino silane, γ-aminopropyltrimethoxysilane ($H_2NC_2H_4NHC_3H_6Si(OCH_3)_3$). This coating was to enhance adhesion between syntactic foam/epoxy and the aluminum ligaments whereas the former produced a weaker adhesion between polymer and metal phases of the IPC foam. Some of the relevant properties of different phases of the IPC foam are listed in Table 1.

Table 1
Properties of constituents.

Properties	Neat epoxy[a]	Microballoons[b]
Elastic modulus (MPa)	3200	–
Bulk density (kg/m^3)	1175	125
Poisson's ratio	0.34	–

[a] Supplied by Beuhler, Inc., under the trade name 'Epo-Thin'.
[b] Supplied by 3 M Corp., under the trade name K-1 microballoons.

2.3. Microstructure

SEM images of polished surfaces of syntactic foam and IPC foam with 30% volume fraction of microballoons are shown in Figs. 2 and 3, respectively. Fig. 2 shows random but uniform distribution of microballoons in the epoxy matrix. From the micrograph it can also be seen that microballoons show a relatively broad size variation. The cross-section of cast cylindrical IPC foam so obtained is shown in Fig. 3(a). The photograph reveals aluminum cell walls (shiny gray ligaments) interconnecting pockets (white) of syntactic foam throughout. A micrograph of an undeformed IPC foam specimen obtained using a scanning electron microscope is shown in Fig. 3(b). It clearly shows aluminum ligaments surrounded by microballoons dispersed in the epoxy matrix. The metal–polymer foam interfaces are crisp and continuous suggesting a good bond between the two. The microstructure does not show any evidence of distortions in the aluminum ligaments caused by the curing process.

3. Compression tests and results

A series of compression tests were carried out on syntactic and IPC foam specimens at room temperature using a MTS universal testing machine fitted with a 100 kN load cell. The tests were performed according to ASTM standard D-695 for plastics. A cross-head speed of 1.25 mm/min was used during the tests done in displacement control mode. Dry graphite powder was used as a lubricant between the platens and the specimen surfaces to minimize friction.

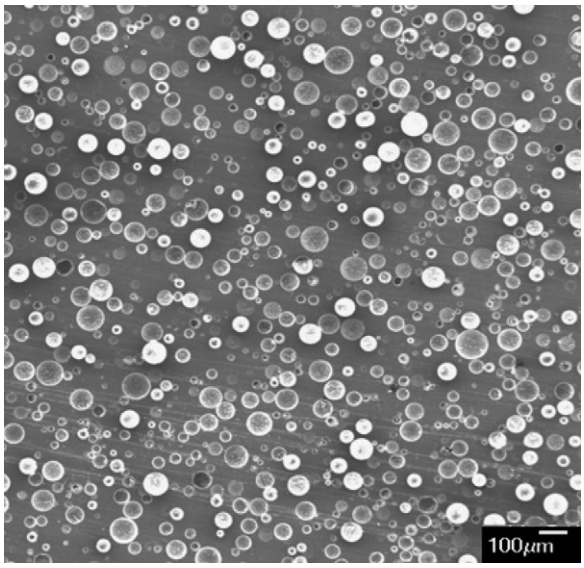

Fig. 2. Micrograph of epoxy syntactic foam with 30% V_f of hollow glass microballoons (mean diameter 60 μm and 0.6 μm thickness).

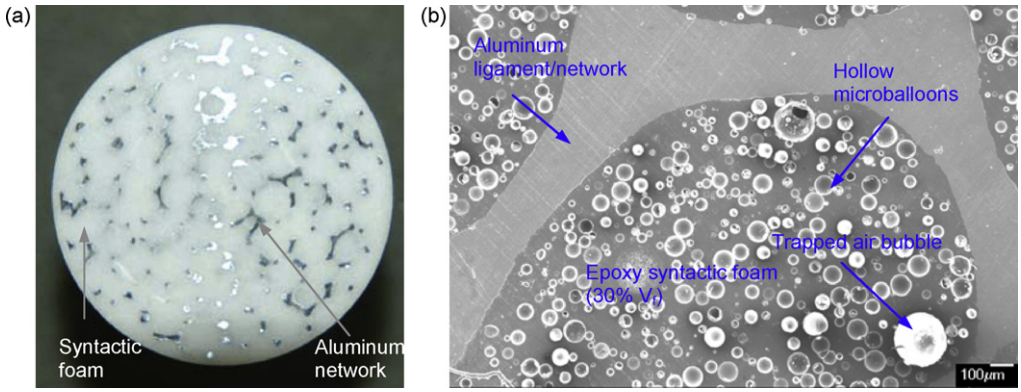

Fig. 3. (a) Cross-section of a lightweight IPC foam cylinder with open-cell aluminum preform (9% relative density) infiltrated with epoxy-based syntactic foam. (b) Micrograph of the IPC foam showing the constituents.

3.1. Syntactic foams

First, uniaxial compression tests were performed on syntactic foam samples of two different specimen length (L) to diameter (D) ratios—0.74 and 0.85. (The aspect ratio was altered by changing the length of the specimen while keeping the specimen diameter same.) The measured engineering stress–strain responses[1] for syntactic foam specimens with 20% microballoon volume fraction and two aspect ratios are shown in Fig. 4(a). The two curves closely overlap on each other and are in close agreement. The value of elastic modulus in each case is 1594 ± 50 MPa and compressive yield stress is 55.7 ± 2 MPa. The results being nearly the same for both the cases, the effect of the two L/D ratios is insignificant for $L/D < 1$ and hence in all subsequent tests a L/D ratio of 0.74 was used. A similar observation has been made by Song et al. [18] who note that increasing the L/D ratio to 2 resulted in a lower compressive strength of the syntactic epoxy foams by ~4.5%. They attributed this reduction to size-dependent defect distribution in their specimens. For this reason $L/D < 1$ was used during this study. A detailed study of the effect of aspect ratio on the failure behavior and compressive properties of syntactic foam has also been reported by Gupta et al. [19].

Next, the repeatability of compressive stress–strain responses of syntactic foam samples was studied. In Fig. 4(b), engineering stress–strain curves for three different samples made from 20% volume fraction of microballoons in epoxy resin is shown. Good repeatability is evident from the figure. (Similar tests for two other volume fractions namely 30% and 40% were also carried out and are not shown here for brevity.) In these curves a linear elastic response is seen initially. Upon yielding, the compressive stress decreases with increasing strain as evident from the softening response following the yield stress. This is followed by a plateau of nearly constant stress where progressive crushing of microballoons occurs. Further increase in load results in densification seen as the region of monotonically rising stress, consistent with the observations reported in the previous works [18–20] on syntactic foams and has many similarities with the compression response of structural foams in general.

The influence of volume fraction (V_f) of microballoons on stress–strain response of syntactic foam was also studied. A few representative stress–strain responses for three V_f – 20%, 30% and 40% – are shown in Fig. 5. An increase in volume fraction of microballons resulted in a reduction of elastic modulus as well as the compressive strength (see Table 2). The elastic modulus and compressive strength decreased from 1595 MPa and 55.7 MPa, respectively for 20% volume fraction case to 1260 MPa and 36.7 MPa for 40% volume fraction case. The foam samples SF-20 ($V_f = 20\%$), SF-30 ($V_f = 30\%$) and SF-40 ($V_f = 40\%$) show a linear elastic response up to strains of approximately 0.028, 0.031 and 0.039, respectively. The plateau stress values in the three cases are 42 MPa, 33 MPa and 27 MPa for SF-20, SF-30 and SF-40, respectively. That is, the plateau

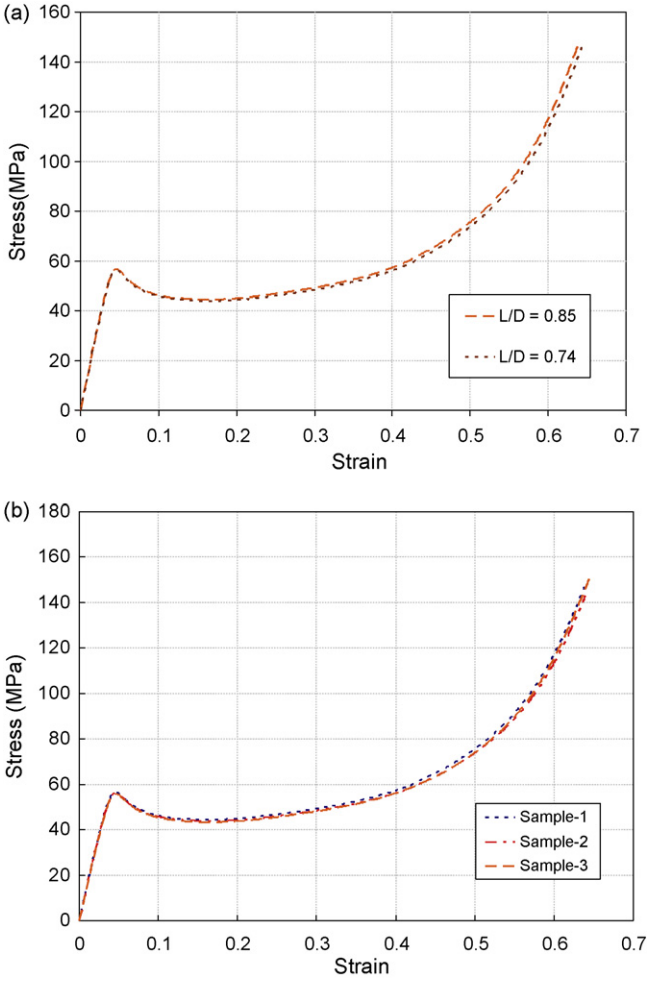

Fig. 4. Stress–strain curves of syntactic foam with 20% volume fraction (a) for two different aspect ratios and (b) for three samples having $L/D = 0.74$.

[1] It is interesting to note that unlike conventional cellular structures and honeycombs, macro scale stress–strain responses for syntactic foams tend to be rather smooth due to microscopic porosity.

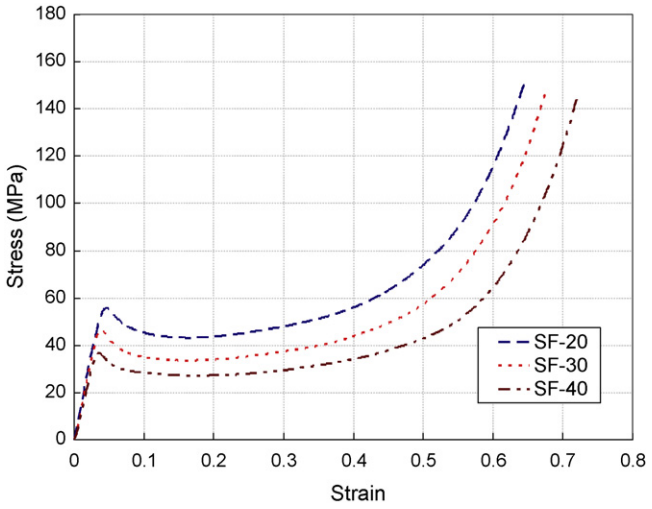

Fig. 5. Stress–strain curves of syntactic foam (SF) with different volume fraction (20, 30, and 40) of microballoons.

stress decreases with increasing volume fraction of microballons and is consistent with the trends reported by Kim and Plubrai [20]. The onset of densification for the three cases is in the strain range of 0.3–0.5 with the lower value corresponding to the lower volume fraction of microballoons. Beyond this strain, stress increases with increasing strain. All specimens showed formation of inclined cracks at advanced stages of loading suggesting shear localization. This is consistent with the previously published results [19,21] for syntactic foams.

In order to explain the failure behavior of syntactic foams, deformed specimens were sectioned and microscopically examined at a few select strain levels. Fig. 6 shows SEM images of a syntactic foam sample (with 30% volume fraction of microballoons). In these, the direction of compression is along the vertical axis. In Fig. 6(a) and (b) micrographs of deformed specimens at 10% and 60% strain are shown. In Fig. 6(c) an enlarged view of an isolated crushed microballoon, highlighted in Fig. 6(b) is shown. It can be clearly seen from the images that the initial softening response is due to the onset of crushing of microballoons. A good interfacial bonding between microballoons and matrix has produced clearly visible fragments of a crushed microballoon adhering to the surrounding matrix. This suggests that interfacial debonding between microballoons and matrix is not a major contributor in the observed global material response shown in Fig. 5. A bias in the direction of fractured microballoons at lower levels of deformation can be seen in Fig. 6(a). With further deformation of the sample, microballoons fracture completely, leading to the densification response seen in the stress–strain curve. Failure of microballoons along inclined planes (relative to the loading direction) also indicates shear localization.

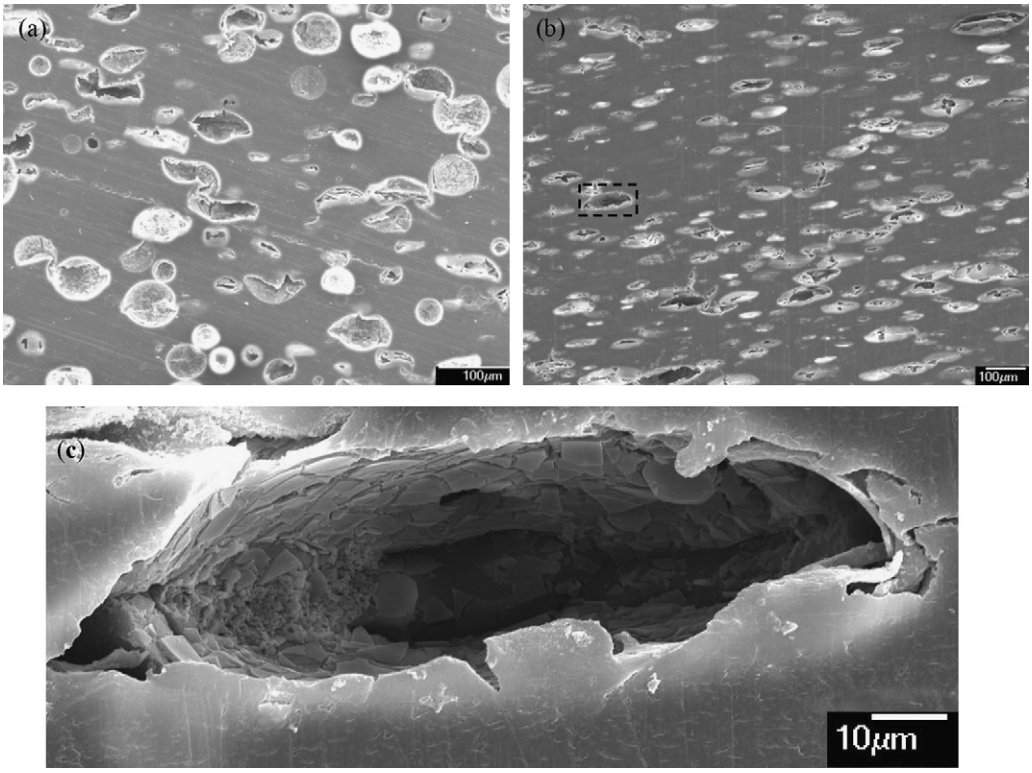

Fig. 6. SEM images of a deformed syntactic foam sample with 30% V_f of microballoons (a) at a strain of ~10%, (b) at a strain of ~60%, and (c) higher magnification image showing fractured surface of a microballoon highlighted by the dotted box in (b). (The sample is compressed in the vertical direction.)

Table 2
Properties of syntactic foam.

Foam designation	Volume fraction of microballoons (%)	Density (kg/m^3)	Compressive strength (MPa)	Elastic modulus (MPa)
SF-20	20	931 ± 4	55.7 ± 2.2	1594.7 ± 35
SF-30	30	821 ± 6	46.3 ± 1.4	1447.6 ± 28
SF-40	40	701 ± 4	36.7 ± 1.8	1260.5 ± 42

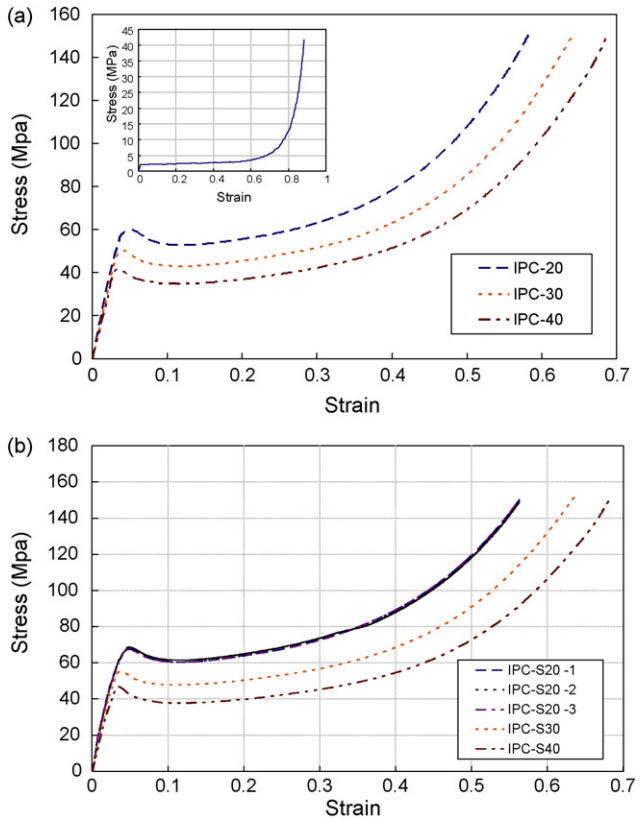

Fig. 7. Compression response of IPC foam: (a) uncoated (b) silane coated. (Data for three specimens are shown for IPC-S20 case to show experimental repeatability.) Stress–strain response of unfilled aluminum preform is shown as an inset in Fig. 7(a). Notice the plateau stress for the preform is ~2.5 MPa.

3.2. IPC foam

Fig. 7 shows typical stress–strain curves for different IPC foam samples. These plots correspond to samples made of aluminum preform infiltrated with syntactic foam containing 20%, 30% and 40% volume fractions of microballoons. Fig. 7(a) shows responses for IPC foam samples when the aluminum preform was used in 'as-is' (uncoated) conditions whereas plots in Fig. 7(b) are for IPC foam counterparts with silane treated preforms. (The inset in Fig. 7(a) corresponds to the compression response of un-infiltrated preform/scaffold. It is shown for comparative purposes and will be discussed later on.) In Fig. 7(b) three results for one particular type of IPC foam (20% syntactic foam with silane treated preform) are shown to demonstrate a high degree of repeatability of these tests. The overall response of IPC foam has similarities with the ones obtained for pure syntactic foam specimens (Fig. 5). These plots (Fig. 7) also show three distinct regions typical of a foam behavior. Initially there is a linear elastic response. The stress plateau region following the onset of nonlinearity is characterized by progressive bending of aluminum ligaments of the IPC foam. This in turn results in crushing of microballons present in between the ligaments of aluminum preform. SEM images of silane coated IPC foam (with 30% volume fraction of microballoons and sample compressed in the horizontal direction) shown in Fig. 8(a) supports this observation. With further increase in load the stress increases more rapidly (compared to syntactic foam samples, Fig. 5). This can be explained by the micrograph in Fig. 8(b) (compression is along the vertical direction) where compaction of crushed microballoons and deformation of aluminum preform is clearly evident. The behavior is dependent on many factors among which the density (dependent on the volume fraction of the microballoons in the current IPC foam) of the composite being the most important. The SEM image in Fig. 8(c) is that of an uncoated IPC foam compressed to about 14% strain. It clearly reveals the effect of weaker adhesion between the metal and polymer phases as evident from an isolated debond highlighted in the micrograph. Such debonds are generally absent even at relatively high strain levels when silane coated preform is used (see Fig. 8(b)).

For comparison, the compression response of an unfilled aluminum preform [22] is shown as an inset in Fig. 7(a). It shows an elastic modulus of ~93 MPa and a plateau stress of ~2.5 MPa without any noticeable softening at the onset of cell collapse. This is

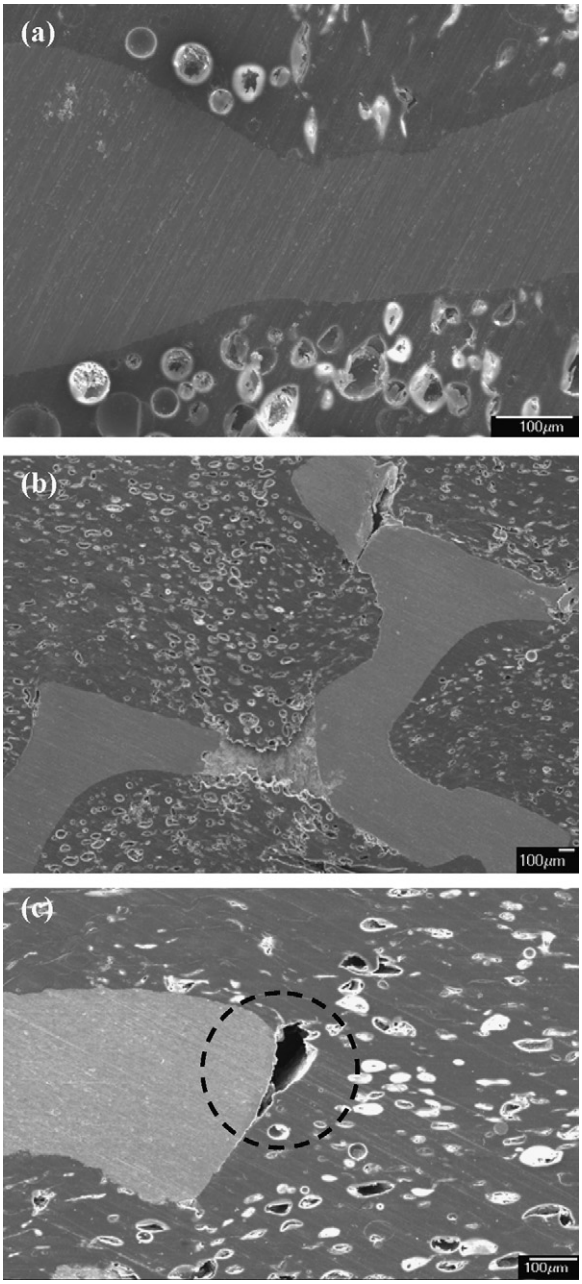

Fig. 8. SEM images of (a) silane coated IPC foam at a strain of 10%, (b) silane coated IPC foam at a strain of 58%, and (c) uncoated IPC foam at a strain of 14%. (Compression is in the *horizontal* direction in (a) and in the *vertical* direction in (b) and (c). In case of uncoated IPC foam, evidence of debonding between the metal preform and syntactic foam can be seen.)

Table 3
Properties of IPC Foam (20, 30, 40 designation denotes V_f of microballoons in the syntactic foam).

IPC foam with uncoated preform				IPC foam with silane coated preform			
IPC designation	Density (kg/m^3)	Compressive strength (MPa)	Elastic modulus (MPa)	IPC designation	Density (kg/m^3)	Compressive strength (MPa)	Elastic modulus (MPa)
IPC-20	1008 ± 12	59.9 ± 2.5	1821 ± 17	IPC-S20	1036 ± 13	67.5 ± 2.3	2123 ± 32
IPC-30	937 ± 8	50.5 ± 1.8	1573 ± 12	IPC-S30	954 ± 12	55.4 ± 3.6	1852 ± 27
IPC-40	861 ± 12	41.5 ± 2.6	1442 ± 28	IPC-S40	879 ± 18	45.8 ± 1.9	1702 ± 26

unlike the response of syntactic foams (see Fig. 5) which have a noticeable softening at the onset of nonlinearity. When responses of pure syntactic and IPC foams with the same volume fraction of microballoons (Fig. 9) are compared, IPC foams show an increase in the plateau stress by as much as 15–20 MPa (depending upon the volume fraction of the microballoons in the infiltrated syntactic foam), much higher than that expected from the aluminum preform. *Synergistic mechanical constraint between aluminum ligaments of the preform and pockets of infused syntactic foam are responsible for this favorable response*. That is, aluminum ligaments are laterally supported by the syntactic foam pockets preventing them from premature bending/buckling as in an unfilled preform. On the flip side, pockets of syntactic foam are reinforced by the metallic ligaments against an early collapse of microballoons.

Another interesting comparison between the responses of IPC foam with silane coated and uncoated aluminum ligaments can be made from Fig. 9(a)–(c). The characteristics, such as yield stress, plateau stress and compaction response, seem to favor silane coated IPC foam over uncoated IPC foam and pure syntactic foam, in that order. This is largely attributed to the elimination of microscopic debonds between aluminum ligaments and syntactic foam as deformation progresses in case of coated IPC foam.

The elastic modulus of the composite was determined using the initial linear portion of the measured stress–strain curves. The elastic modulus and the upper yield stress for IPC foam made from uncoated and coated aluminum preforms are quantified in Table 3 and are found to monotonically decrease with increasing volume fraction of microballons in the syntactic foam. This behavior is consistent with the corresponding values of pure syntactic foam (see Table 2). From Table 3 it can also be noted that the elastic modulus and yield stress of IPC foam with silane coating is higher when compared with the corresponding uncoated preform for all volume fractions of microballoons in syntactic foam. As noted earlier, the increase in elastic modulus and compressive strength of silane coated preform can be attributed to improved wettability, which in turn enhances adhesion between the metal and polymer phases. The IPC foam is also found to have improved mechanical properties when compared with those for the respective syntactic foams.

In Fig. 9(a)–(c), data for syntactic foam and the corresponding IPC foam samples with uncoated and silane coated preforms is examined comparatively for 20%, 30% and 40% volume fraction of microballoons. There is a substantial increase in all the relevant characteristics of IPC foam when compared to that for pure syntactic foam samples. The increase in elastic modulus for IPC foam with silane coated preform was found to be 33%, 28%, and 35% for the composite IPC-S20, IPC-S30, IPC-S40, respectively when compared to the *corresponding* pure syntactic foam. (The *corresponding increases* can be assumed to be nearly constant after factoring experimental scatter in the data into account.) The relative increase in the compressive strengths for the three composites were 21.2%, 19.7%, and 24.8%, respectively, relative to the *corresponding* syntactic foam samples. From Fig. 9 it can also be seen that treating aluminum preforms with silane results in an increase in plateau stress for the same three IPC foams when compared to the uncoated versions IPC-20, IPC-30 and IPC-40, respectively. Also the percent-

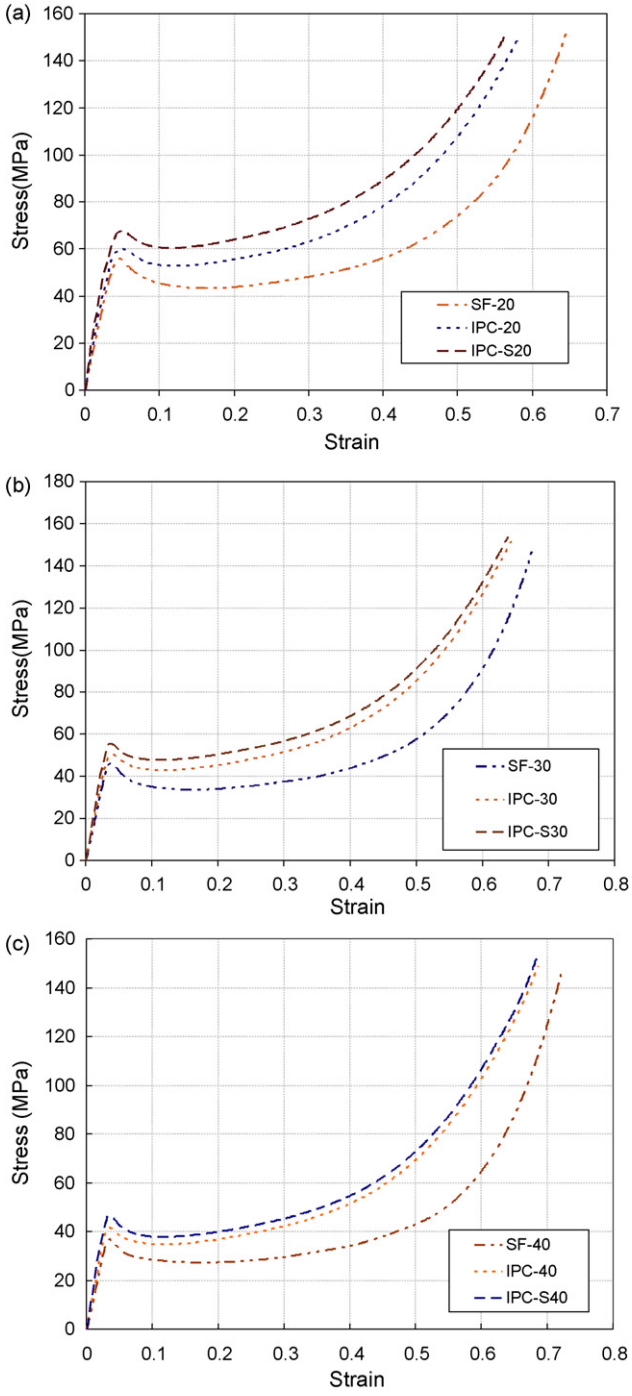

Fig. 9. Comparison of stress–strain response of syntactic foam, IPC foam with uncoated preform and IPC foam with silane coated preform for (a) 20% volume fraction, (b) 30% volume fraction, and (c) 40% volume fraction of microballoons. Notice the increase in the plateau stress (by ~15–20 MPa) of silane treated IPC foam in each case is well above the plateau stress (~2.5 MPa) of unfilled preform shown in Fig. 7(a).

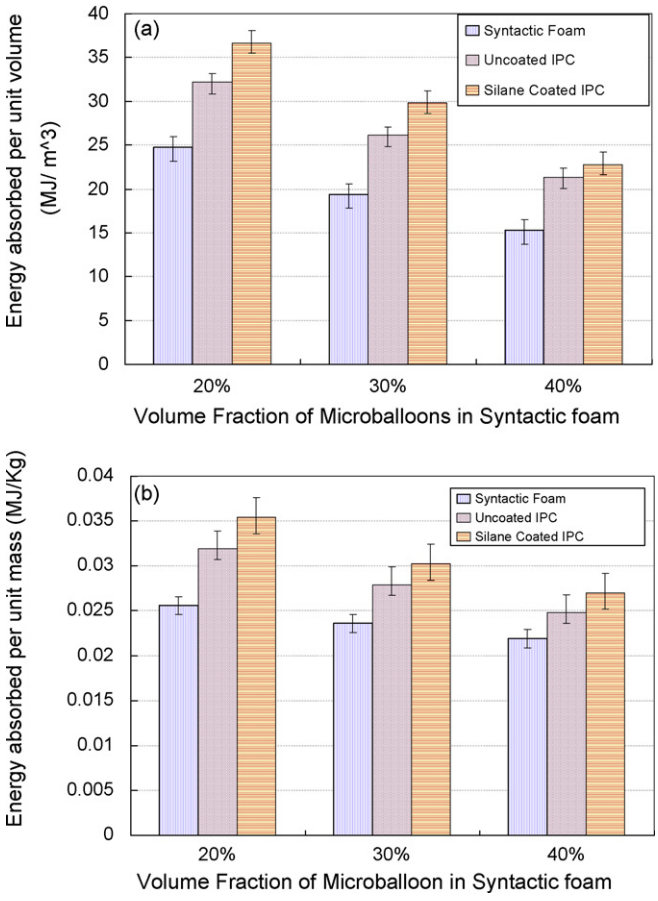

Fig. 10. Comparison of energy absorption (up to 50% strain) for syntactic foams and IPC foam samples: (a) per unit volume and (b) per unit mass.

age increase is a maximum for IPC-S20 which is approximately 14% and it decreases with increasing volume fraction of microballoons to a value of about 8% for IPC-S40.

4. Energy absorption

Conventional cellular materials have found application in automotive and packaging industries due to their excellent energy dissipation characteristics. The cellular structure of these materials enables them to undergo large deformations in compression, enabling them to absorb considerable amounts of energy [12]. Thus improvements in energy absorption achieved by IPC foam samples when compared to the corresponding syntactic foam counterparts needs to be highlighted. The energy absorbed per unit volume (U) can be found by evaluating the area under the stress–strain curve

$$U = \int_0^{\varepsilon} \sigma(\varepsilon)\,\mathrm{d}\varepsilon \tag{1}$$

where $\sigma(\varepsilon)$ denotes uniaxial stress as a function of strain. The energy absorbed up to 50% strain is plotted as histograms in Fig. 10. The syntactic foam with 20% (SF-20) volume fraction of microballoons is found to have the highest value of energy absorption when compared to 30% (SF-30) and 40% (SF-40) cases, in that order. Similar trend can also be seen for IPC foam with silane coated and uncoated aluminum preform. Approximately 50% increase in the absorbed energy per unit volume of silane coated IPC foam samples relative to the conventional syntactic foam is evident from Fig. 10(a). Specifically, 48%, 53% and 49% increase in the absorbed energy per unit volume for IPC-S20, IPC-S30 and IPC-S40 relative to the conventional syntactic foam samples SF-20, SF-30 and SF-40, respectively, is indicative of the potential of IPC foams for energy dissipation applications. On the other hand, when IPC foam samples had an uncoated preform, the absorbed energy was modestly lower and was found to be 31%, 37% and 40% for IPC-20, IPC-30 and IPC-40 relative to SF-20, SF-30, and SF-40, respectively. Introduction of aluminum preform increases the overall weight of the composite and hence specific energy absorption (energy absorbed per unit mass) was also calculated. From Fig. 10(b), the increase in the value of specific energy absorption per unit mass for IPC-S20 is found to be about 33% when compared to the corresponding syntactic foam case (SF-20). This value decreases to about 28% and 23% for IPC-S30 and IPC-S40 when compared to syntactic foam cases SF-30 and SF-40, respectively. This also shows that with increasing volume fraction of microballoons in syntactic foam, the percentage increase in the value of specific energy absorption reduces. From stress–strain plots shown in Fig. 9 for various volume fractions of microballoons in syntactic foam, it can be seen that coating the aluminum preform with silane results in improved compression characteristics of the IPC foam resulting in higher values of compressive strength and elastic modulus relative to the uncoated IPC foam. There is also an increase in energy absorption per unit mass of IPC foam with silane coated aluminum preform when compared to the uncoated preform and is found to vary between 11% and 9% with decreasing volume fraction of microballoons.

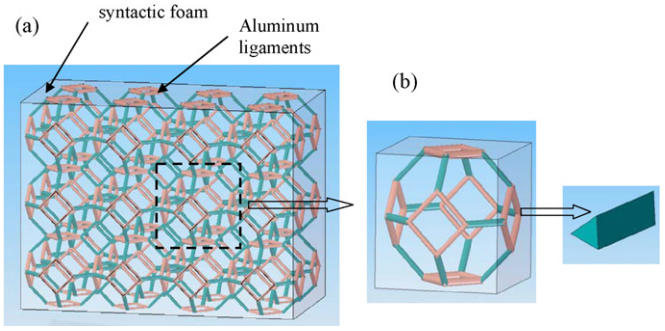

Fig. 11. Finite element model development: (a) Idealization of IPC foam structure using Kelvin cells. (b) Unit cell model used to represent aluminum-syntactic foam IPC.

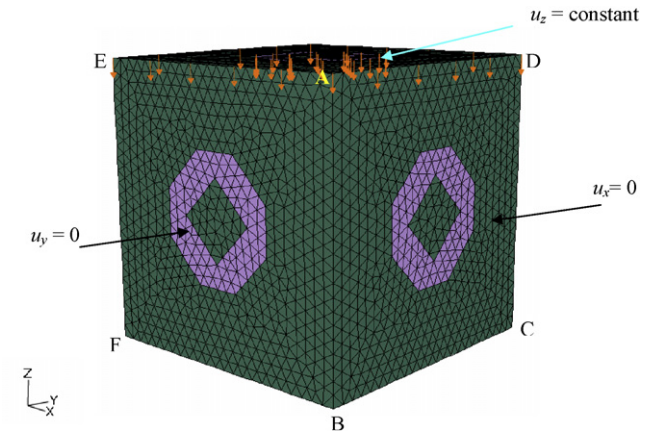

Fig. 12. Finite element model of undeformed unit cell with boundary conditions used while simulating the uniaxial compression of IPC foam. (Different colors/shades show metallic ligaments embedded in the syntactic foam cubic cell.). (For interpretation of the references to color in this figure legend, the reader is referred to the web version of the article.)

Table 4
Comparison of finite element results with experiments (based on true stress–strain data).

IPC designation	Finite element results			Experimental results		
	Elastic modulus (MPa)	Compressive strength (MPa)	Plateau stress (MPa)	Elastic modulus (MPa)	Compressive strength (MPa)	Plateau stress (MPa)
IPC-S20	2204	67.8	52.0	2109	64.2	50.8
IPC-S30	1938	55.8	41.9	1843	53.2	40.2
IPC-S40	1792	47.9	33.7	1689	45.0	31.7

5. Finite element modeling

In order to model stress–strain characteristics of IPC foams finite element method was utilized and the results were validated by those obtained from experiments discussed earlier. To understand the mechanical behavior of the IPC foam on hand, it would be appropriate to consider models with randomly interpenetrating 3-D structures, similar to the one studied experimentally. However, in view of practical considerations of modeling the complexities of the metallic preform and syntactic foam, a unit cell based analysis was carried out.

In order to represent the open-cell foam microstructure, previous structural foam researchers [23–25] have successfully used space filling Kelvin cells [26]. These investigators have vividly demonstrated the ability of these cells and finite element method to capture the behavior of open-cell foams. A Kelvin cell is a tetrakaidecahedron, a 14-sided polyhedron comprised of six squares and eight hexagonal faces. In the present work, initial modeling of a Kelvin cell was done using solid modeling software SOLIDEDGE®. The actual cross-section of aluminum ligaments of the preform/scaffold used in experiments was close to a triangular shape and hence was approximated as an equilateral triangle in the simulations for simplicity. The space inside and outside this cell was filled with syntactic foam, assumed to be a macroscopically homogeneous and isotropic solid medium for modeling purposes. This results in an interpenetrating structure, representative of the IPC foam on hand. The unit cell model used to represent the IPC foam is shown in Fig. 11. All ligaments of the Kelvin cell have the same length (L) and the cell height in this case is $h = 2\sqrt{2}\,L$. The cross-sectional area of the ligaments was decided such that the overall volume fraction of the aluminum foam in the IPC foam is approximately 9%, same as that of the preform used in the experiments.

Finite element analyses were carried out using ABAQUS/standard structural analysis software. A four node tetrahedron element (element type C3D4) in ABAQUS with linear interpolation was used to discretize the unit cell. The unit cell model has a total of 86865 elements and 16111 nodes.[2] The elastic constants of aluminum and the respective syntactic foam (from experiments) were assigned to the two phases of the IPC foam. The plasticity model based on associated plastic flow and von-Mises yield criterion with isotropic hardening was used to model plasticity of both metallic and syntactic foam phases. In the associated plastic flow rule the direction of flow is the same as the direction of the outward normal to the yield surface and in isotropic hardening the yield surface is assumed to maintain its shape, while its size increases or decreases as plastic straining occurs. Since the applied strains were greater than the elastic limit (~40% in this work), geometrical nonlinearity was also incorporated into the analysis. The stress–strain response of aluminum Al6101-T6

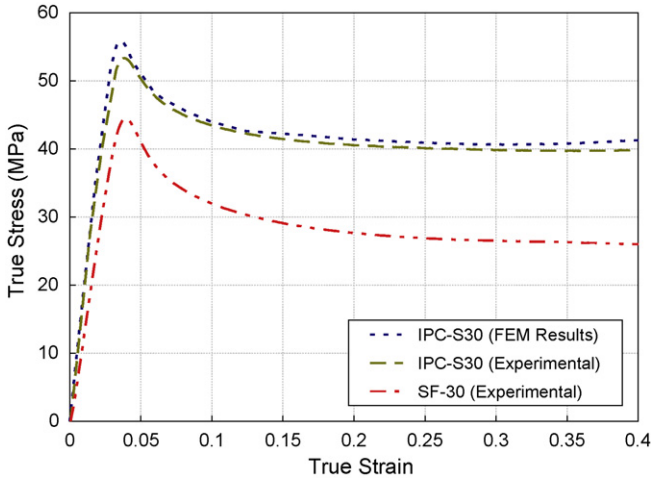

Fig. 13. Comparison of numerical and experimental results for IPC foam with 30% volume fraction of microballoons. Experimental result for the corresponding conventional syntactic foam is also shown for comparison.

(Young's modulus = 69 GPa, $\nu = 0.35$, yield stress = 172 MPa at 0.2% strain and ultimate stress = 200 MPa (at 15% strain) based on Alcoa Inc. datasheet) was assigned to all the elements representing the metallic ligaments. Measured stress–strain responses for syntactic foams made with different volume fractions of microballoons were used to model the infiltrating material surrounding the ligaments of the unit cell. The model was subjected to uniaxial compression by displacing the nodes uniformly on the top face of the cell in the z-direction, as shown in Fig. 12. The nodes on the other lateral faces of the unit cell were constrained in the respective outward directions but were free to displace in the in-plane directions.[3] All the prescribed boundary conditions are shown in Fig. 12, where displacements of nodes on the face ABCD along the x-direction is zero and similarly displacements of nodes on the face ABEF along the y-direction is zero.

5.1. Results and discussions

The uniaxial compressive behaviors of IPC foam with different volume fractions of microballoons (20%, 30% and 40%) in syntactic foam were simulated and the results were compared with the corresponding ones from experiments. In Fig. 13, the finite element results for IPC foam with 30% volume fraction of microballoons in syntactic foam are compared with experimentally obtained true stress–strain response. The measured stress–strain response of syntactic foam with 30% volume fraction of microballloons is also shown for comparative purposes. It can be seen that the simula-

[2] A mesh convergence study was performed using different element sizes (average sizes—0.0825 mm, 0.152 mm and 0.325 mm) and it was found that the element size of 0.152 mm was sufficient for achieving convergence, and hence was used in all the simulations. The details are avoided here for brevity.

[3] Previous foam mechanics researchers have used either displacement constraints or periodic boundary conditions in their studies. As a first step to study IPC foam, the former approach was adopted here due to its simplicity. The validity of the model was assessed based on its agreement with measurements, as discussed in sub-section 5.1.

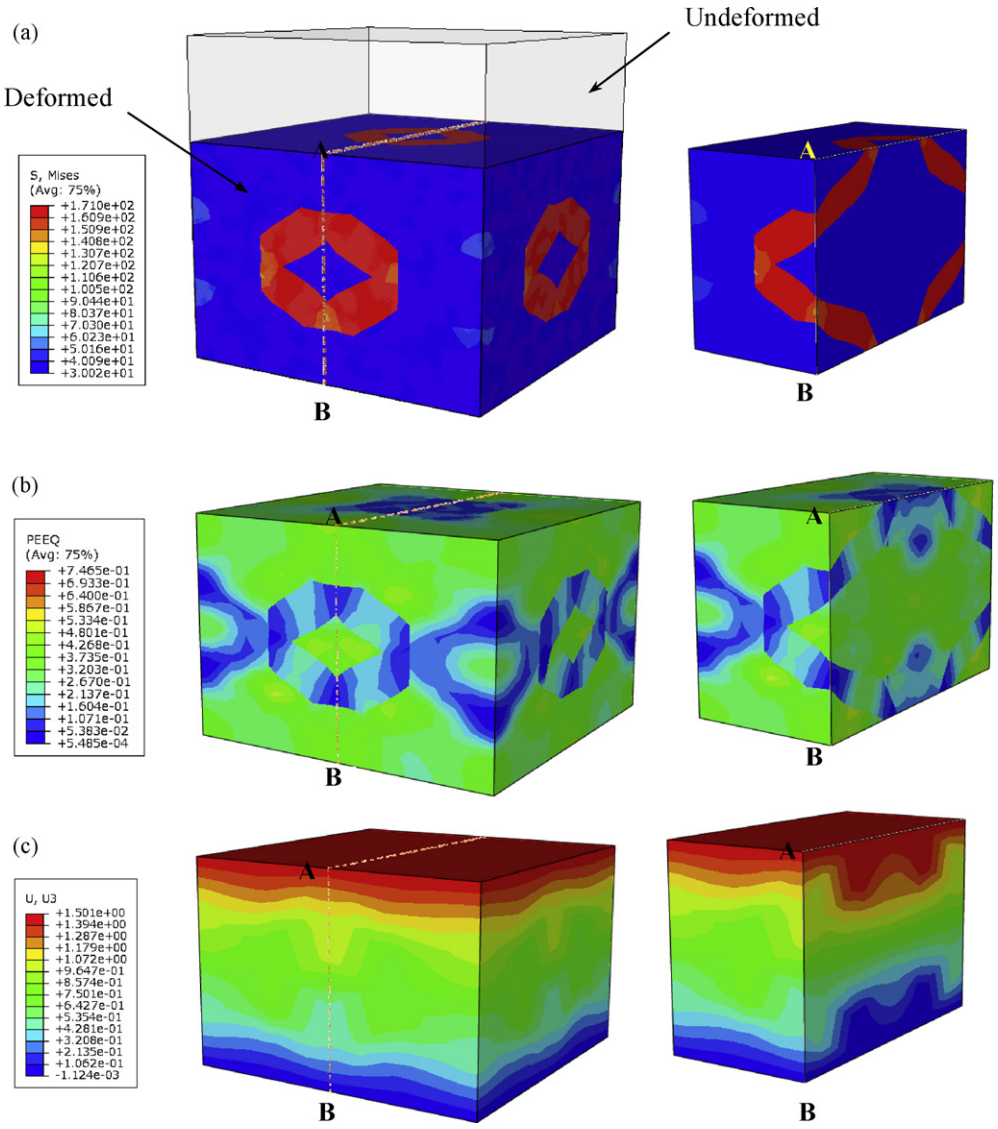

Fig. 14. Finite element results for unit cell model for IPC-S30 at 40% strain. (a) Deformed and undeformed unit cell with von-Mises stress contours. (b) Deformed unit cell with equivalent plastic strain contours. (c) Deformed unit cell with displacement contours in the u_3 (u_z).

tions indeed capture the measured IPC foam behavior very well. In the post-yield regime, the simulations seem to slightly over predict the measurements attributed primarily to the idealization of uniform and defect free bonding between aluminum and syntactic foam phases. The assumption of uniform cross-sectional area for all ligaments throughout the unit cell could be an additional contributor to this over prediction. The experimental data and simulation results for IPC-S20 and IPC-S40 had a similar agreement and are not shown in favor of brevity. Table 4 lists the values of elastic modulus, compressive strength and plateau stress of the IPC foam obtained from finite element simulations for all the three cases. Again, from the results it is evident that the predictions are slightly higher in all cases when compared to measurements.

A few representative results from finite element simulations for IPC-S30 case are shown in Fig. 14(a)–(c). In Fig. 14(a), von-Mises stress contours are depicted on the unit cell and on an interior planar section denoted by A and B at an imposed strain of 40%. As expected, the ligaments experience higher stresses compared to the surrounding syntactic foam. From the contours of equivalent plastic strain (Fig. 14(b)) it can be seen that the strain levels are higher for the syntactic foam when compared to that in the aluminum phase as syntactic foam has lower yield strength when compared to the preform ligaments. Further, non-uniformity of strains through the cross-section of the unit cell is clearly evident. In Fig. 14(c), displacement contours in the direction of the imposed strain (u_3) is shown. The presence of aluminum ligaments in the unit cell clearly perturbs the uniformity of displacements as evident by the contours on and within the cell.

6. Conclusions

The feasibility of processing lightweight interpenetrating phase composite (IPC) foams using aluminum open-cell preforms/scaffolds and syntactic polymer foam is demonstrated. The structural composite foam is produced by infiltrating uncured epoxy-based syntactic foam containing micron-size hollow glass microballoons into aluminum open-cell preform of millimeter size cavities. The cured product forms a meso-/micro-scale IPC foam with promising compression characteristics. Different IPC foam varieties are processed by varying the volume fraction of microballoons from 20% to 40% in the syntactic foam. Two variants of these

IPC foams are produced by using aluminum preform in 'as-is' condition and by coating it with silane to increase adhesion between the metal scaffold and polymer foam.

Cylindrical IPC foam specimens are tested in uniaxial compression and failure responses are examined relative to the conventional syntactic foam with the corresponding volume fraction of microballoons. The IPC foam samples show stress–strain responses similar to the ones for conventional structural foams. An initial linear elastic response is followed by a noticeable softening caused by the onset of collapse of microballoons leading to a plateau stress and compaction behaviors are seen. IPC foam samples in general and the silane coated ones in particular show improvement in elastic modulus, compression strength and plateau stress values by 28–35%, 20–25%, and 37–42% respectively, when compared to conventional syntactic foam with the same volume fraction of hollow microballoons. More importantly, the increase in plateau stress of IPC foam samples by 15–20 MPa relative to the corresponding syntactic foam samples is significantly higher than the plateau stress of ~2.5 MPa for an unfilled preform. This is attributed to synergistic mechanical constraint between the syntactic foam and aluminum preform of the IPC foam. This also produces a rather pronounced improvement in the energy absorption in IPC foam relative to the corresponding syntactic foam samples. Approximately 50% higher energy absorption per unit volume and 33% higher energy absorption per unit mass relative to the corresponding syntactic foam is realized in silane treated IPC foam. When preforms are untreated, the percentage increase in energy absorption is somewhat lower.

A Kelvin cell based 3-D elasto-plastic finite element model is developed by adopting unit cell analysis approach to examine the feasibility of predicting both the elastic and plastic characteristics of the IPC foam. This analysis is aimed at validating the case of silane treated preform where adhesion between the ligaments and foam can be assumed to be relatively strong. The numerical model based on measured compression response of the corresponding syntactic foam and aluminum is able to successfully capture the overall IPC foam behavior.

Acknowledgments

The partial support of this research by the U.S. Army Research Office (Grant #ARMY-W911NF-08-1-0285) is gratefully acknowledged. The authors appreciate the assistance of Mr. Chandru Periasamy in modeling the Kelvin cell for finite element analysis.

References

[1] D.R. Clarke, Journal of the American Ceramic Society 75 (4) (1992) 739–759.
[2] M.C. Breslin, J. Ringnalda, L. Xu, M. Fuller, J. Seeger, G.S. Daehn, T. Otani, H.L. Fraser, Journal of Materials Science and Engineering—A 195 (1995) 113–119.
[3] G.S. Daehn, B. Starck, L. Xu, K.F. Elfishawy, J. Ringnalda, H.L. Fraser, Acta Materalia 44 (1) (1996) 249–261.
[4] A. Imagawa, T.C. Qui, Macromolecules 28 (24) (1995) 8388–8394.
[5] S. Skirl, M. Hoffman, K. Bowman, S. Wiederhorn, J. Rodel, Acta Materalia 46 (7) (1998) 2493–2499.
[6] H. Veenstra, P.C.J. Verkooijen, B.J.J. Van lent, J.V. Dam, A.P. De boer, A.P.H.J. Nijhof, Polymer 41 (2000) 1817–1826.
[7] L.D. Wegner, L.J. Gibson, International Journal of Mechanical Sciences 42 (2000) 925–942.
[8] T. Etter, J. Kuebler, T. Frey, P. Schulzc, J.F. LÖffler, P.J. Uggowitzer, Materials Science and engineering—A 386 (2004) 61–67.
[9] R.J. Moon, M. Tilbrook, M. Hoffman, Journal of American Ceramic Society 88 (3) (2005) 666–674.
[10] H. Mayer, M. Papakyriacou, Carbon 44 (2006) 1801–1807.
[11] Y. Liu, X.-L. Gong, Transactions of Nonferrous Metals Society of China 16 (2006) s439–s443.
[12] L.J. Gibson, M.F. Ashby, Cellular Solids: Structure and Properties, 2nd ed., Cambridge University Press, 2001.
[13] L.D. Wegner, L.J. Gibson, International Journal of Mechanical Sciences 43 (2001) 1061–1072.
[14] A. Mattern, B. Huchler, D. Staudenecker, R. Oberacker, A. Nagel, M.J. Hoffmann, Journal of the European Ceramic Society 24 (2004) 3399–3408.
[15] R.A. Saravanan, M.K. Surappa, Materials Science and Engineering—A 276 (2000) 108–116.
[16] F.A. Shutov, in: D. Klempner, K.C. Frisch (Eds.), Handbook of Polymeric Foams and Foam Technology, Hanser Publishers, New York, 1991.
[17] M.S. Kirugulige, R. Kitey, H.V. Tippur, Composites Science and Technology 65 (2005) 1052–1068.
[18] B. Song, W. Chen, D.J. Frew, Journal of Composite Materials 38 (11) (2004) 915–936.
[19] N. Gupta, Kishore, E. Woldsenbet, S. Sankaran, Journal of Materials Science 36 (18) (2001) 4485–4491.
[20] H.S. Kim, P. Plubrai, Composites Part A: Applied Science and Manufacturing 35 (9) (2004) 1009–1015.
[21] N. Gupta, E. Woldesenbet, Kishore, Journal of Materials Science 37 (2002) 3199–3209.
[22] Material Datasheet, ERG Materials and Aerospace Corporation, USA.
[23] L. Gong, S. Kyriakides, W.Y. Jang, International Journal of Solids and Structures 42 (2005) 1355–1379.
[24] L. Gong, S. Kyriakides, N. Triantafyllidis, Journal of the Mechanics and Physics of Solids 53 (2005) 771–794.
[25] M.H. Luxner, J. Stampfl, H.E. Pettermann, International Journal of Solids and Structures 44 (2007) 2990–3003.
[26] W. Thomson (Lord Kelvin), Philosophical Magazine 24 (5th series) (1887) 503–514.